Transactions of the Materials Research Society of Japan 29[4] 1713-1718 (2004)

Innovative Magnetic Bearing Motor

Chien-Chang Wang, Chau-Shin Jang,
Wei-Chen Cheng, Chien-Sheng Liu, Yu-Hsiu Chang, and Der-Ray Huang
Opto-Electronics & Systems Laboratories, Industrial Technology Research Institute, Taiwan.
Bldg.78, 195 Chung-Hsin Rd., Sec. 4, Chutung, 310, Hsinchu, Taiwan.
Fax: 81-3-591-8095, e-mail: DERRAY@itri.org.tw

ABSTRACT — An innovative DC motor with passive radial magnetic bearing has been developed for low noise and long life span applications. Annular-shaped NdFeB permanent magnets, with axially magnetized are assembled along the shaft and stator in axial direction. To achieve stable state of the magnetic bearing, shaft is in contact with the loading section on a fine designed area. Magnetic axial force and radial force are designed and calculated by finite element analysis (FEA), for supporting a slight radial air gap between rotor and stator. The magnetic bearing motor shows lower running current and higher rotated speed compared with ball bearing type motor. The running current is around 0.28A and the rotated speed is higher than 3840 rpm. The natural frequencies for lateral and rotational modes of the rotor are around 23 Hz. The system resonance is avoided. The natural damping ratio in radial direction of the rotor is 0.0545. The radial run-out obtained is smaller than 100 μm that shows the rotating shaft can be rotated without any frictional contact in radial direction.
Key words: Magnetic bearing, Motor, Passive, Damping, Damping ratio.

I. INTRODUCTION

The bearing is the most important key component of a spindle motor. The life span, vibrations, anti-shock and noises properties of spindle motor are good enough or not depend on the bearing's quality significantly. Generally, in a spindle motor used in a data storage device such as DVD, HDD devices, a ball bearing type spindle motor is broadly used in the driving system. However, it has some disadvantages. Due to the defects of precision of a ball, noise and vibration are created. The seal structure causes the high speed is limited to a certain level, life span is shorten, and it has the low anti-shock properties.

Complicated magnetic bearing structures with conventional axial pivot are applied to spindle motor to improve these performances discussed above [1-4]. Also the special magnetic circuit designs with balancing sheet, which is used to increase the axial preload, to achieve the same objective [5]. The main goal of this paper is to design a simple magnetic bearing system that utilizes two pairs of permanent magnets to replace the two ball bearings. The performance of repulsive magnetic bearing motor will be reported.

II. DESIGN AND SIMULATION

Figure 1 shows the configurations of the magnetic bearing motor. The ratio of slot number to pole number is 4:4. The radial air gap between the stator and the rotor was fixed to 7×10^{-4} m. A Ba-ferrite ring with inner diameter of 3.14×10^{-2} m, axial length of 1.34×10^{-2} m, and outer diameter of 3.94×10^{-2} m were used for the magnetic rotor. Outside of the ferrite ring, an iron yoke with outer diameter of 4.1×10^{-2} m was attached. The magnetic bearing spindle motor was designed under the conditions of the rated speed is 3840 rpm with an unbalance 9.8×10^{-6} Nm of the rotor, the centrifugal force of 0.1617 N is generated and the rated current is 0.28 A.

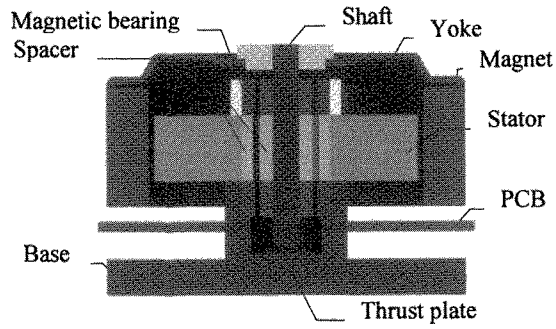

Fig. 1. Magnetic bearing motor.

The outer diameter and inner diameter of a ball bearing are 3×10^{-3} m and 7×10^{-3} m, with axial length 4×10^{-3} m. The magnetic bearing motor is constructed by replacing the pair of ball bearings with a pair of magnetic ones.

Two permanent magnetic annular magnetic rings were mounted on a shaft and two annular magnetic rings were mounted on a stator. The shaft bottom contacted the thrust plate. The magnet geometry was optimized in order to increase the restoring force in radial direction. NdFeB magnets with $(BH)_{max}$ of 45 MGOe were used. The dimensions of the rotating and stationary magnets are as follows. The OD of the rotating magnet is 6×10^{-3} m and the ID is 3×10^{-3} m. The stationary magnet OD is 1×10^{-2} m and ID is 7×10^{-3} m. The thickness of magnet used in both rotor and stator is 4×10^{-3} m. The rotating and stationary magnets had a slight 5×10^{-4} m radial air gap. Both rotating and stationary magnets had the same magnetization direction along axial axis. The axial

distance between upper magnetic bearing and lower one is 7.5×10^{-3} m.

Finite element analysis was used to analyze the magnetic force of the magnetic bearing motor. To design a stable magnetic bearing motor system, there are three terms should be considered.

First, in the static state, the system should be stabilized in all axes when the rotor is tilted at a critical angle defined as Θ along the X-axis. Due to the geometry constrain of the radial air gap is 500 μm and the desired radial run-out should be smaller than 75 μm (peak). The Force analysis is considered, in the critical condition when the Θ is equal to 1° shown as Fig. 2 (b).

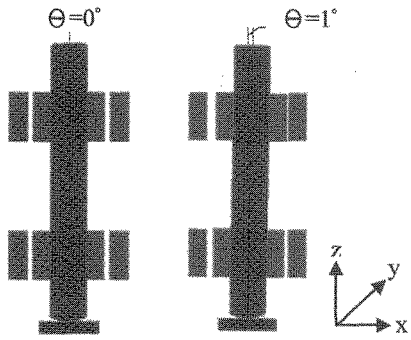

Fig. 2. (a) Rotor is tilted at a critical angle 0° about positive X-axis. (b) Rotor is tilted at a critical angle 1° about positive X-axis.

The restoring torque about Y-axis was defined as T_y and the axial force was defined as F_z. The 3D full model of the finite element analysis was constructed to compute these parameters, as shown in Fig. 3. For each variation of the axial displacement defined as D_{zz} (When the inner magnetic annular is lower than the outer one along the positive Z-axis, it was specified with $D_{zz} > 0$) of inner and outer magnetic annular rings, the rotor was rotated 1° about the Y-axis. Then T_y and F_z were calculated and shown as table I. It was clear that the state of the system with $0 \le D_{zz} \le 3\times10^{-4}$ m was stable.

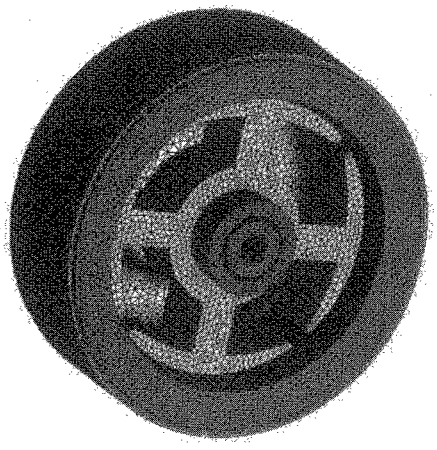

Fig. 3. 3D solid model mesh of the magnetic bearing motor.

Table I T_y and F_z vs. various D_{zz}.

$D_{zz}(10^{-5}m)$	T_y(Nm)	F_z(N)	State
- 10	- 0.01658	2.420	Unstable
0	- 0.01525	- 1.997	Stable
10	- 0.01219	- 4.086	Stable
20	- 0.00788	- 5.719	Stable
30	- 0.00487	- 7.070	Stable

Secondly, in the dynamic state, the system should be stabilized in all axes when the rotor is loading the unbalance 9.8×10^{-6} Nm, rotated in the rated speed 3840 rpm and the centrifugal force 0.1617N is generated. For supporting the dynamic load (0.1617N), the radial magnetic force is considered two times as it. That is equivalent to 0.3234N. The target of the radial run-out was supposed to be lower than 150 μm (peak to peak) in this prototype. To achieve the stable zone of D_{zz}, whenever the radial displacement was greater than 75 μm, the radial force must be greater than 0.3234 N. Approach to this computation of radial force of the development system, the stator was fixed and the rotor was shifted along the positive X-axis as the following five different positions, 0, 1×10^{-4} m, 2×10^{-4} m, 3×10^{-4} m, 4×10^{-4} m and 4.9×10^{-4} m for each D_{zz}. Three relative positions of magnetic inner and outer ring were shown as Fig. 4. In which Fig. 4 (a-1) showed the radial displacement of the rotor along positive X-axis was 0. Fig. 4 (a-2) showed the displacement of the rotor along positive X-axis was 3×10^{-4} m. And Fig. 4 (a-3) showed the radial displacement of the rotor along positive X-axis was 4.9×10^{-4} m.

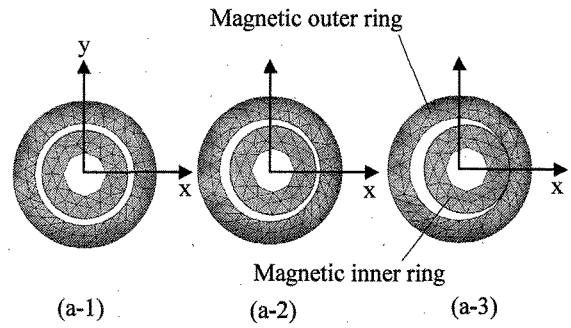

Fig. 4. 2D top view of relative location of the rotor and stator.

From these locations, arrangement of the rotor and stator, the radial force could be obtained as a function of the radial displacement during the force calculation. In order to analyze the radial force as a function of radial displacement at various D_{zz} values, the variation of D_{zz} is chosen as follows 0, 1×10^{-4} m, 2×10^{-4} m, 3×10^{-4} m, and 4×10^{-4} m. And its 3D structure distribution at D_{zz} = 0 was shown as Fig. 5, in which, ①, ②, ③ and ④ showed upper magnetic outer ring, lower magnetic outer ring, upper magnetic inner ring, lower magnetic inner ring respectively. The rotor was shifted along negative axis. Both in Fig. 4 and Fig.5 only the magnetic inner and outer ring were demonstrated.

Both radial force and axial force were known, then the stiffness of the magnetic bearing is perfectly determined. Because of the axial symmetry and the magnetic bearings made exclusively of permanent magnets, the axial stiffness is twice as radial stiffness according to Earnshaw's theorem [6].

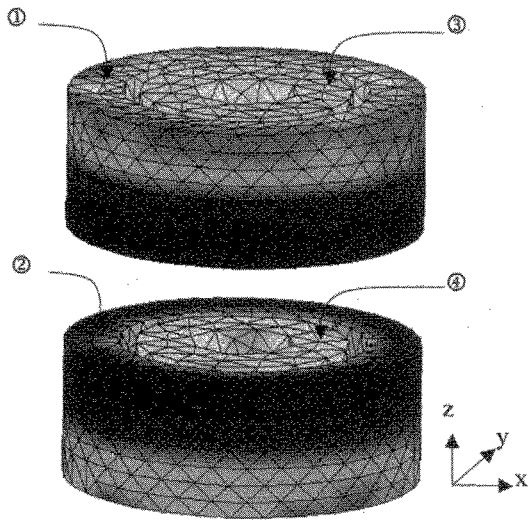

Fig. 5. 3D distribution of rotor and stator.

After computations were performed, we found the value of radial force for each radial displacement. And the radial force as a function of D_{zz} could be obtained. Also, use the same process for F_z as a function of radial displacement was calculated. The final results were presented in Fig. 6 (a) and Fig. 6 (b). Figure 6 (a) shows the radial force as a function of radial displacement of the rotor. The radial force is linearly proportional to radial displacement at $D_{zz} = 0$. Also as the $D_{zz} = 1\times10^{-4}$ m, 2×10^{-4} m, 3×10^{-4} m, and 4×10^{-4} m, the radial force vs radial displacement have the same characteristic, except the radial displacement is greater than 4×10^{-4} m. Graphically the equation Fr = - 0.3234 N and radial displacement = 75 μm give two lines A and B, as shown in Fig. 6 (a). It is manifest that in the fourth quadrant of line A crosses line B, the Fr is greater than the rated load whenever the radial displacement is greater than 75 μm. From the data analysis of radial force and the results of table I, it indicates that the stable zone of D_{zz} is between 0 and 3×10^{-4} m. The rotor can be levitated in the radial direction without any frictional contact when the radial run-out (peak to peak) is less than 150 μm. Figure 6 (b) shows the axial force as a function of radial displacement of rotor. The number of axial force at D_{zz} = 0 was around zero from radial displacement = 0 to 4.9×10^{-4} m. For a fixed value of D_{zz}, the axial force rose slowly in the same radial displacement scope. For a fixed value of radial displacement of rotor, the axial force increased with increasing D_{zz}. The axial force of the magnetic bearing motor with radial displacement = 4.9×10^{-4} m increase from 0 N for D_{zz} = 0 to - 6.543 N for $D_{zz} = 4\times10^{-4}$ m.

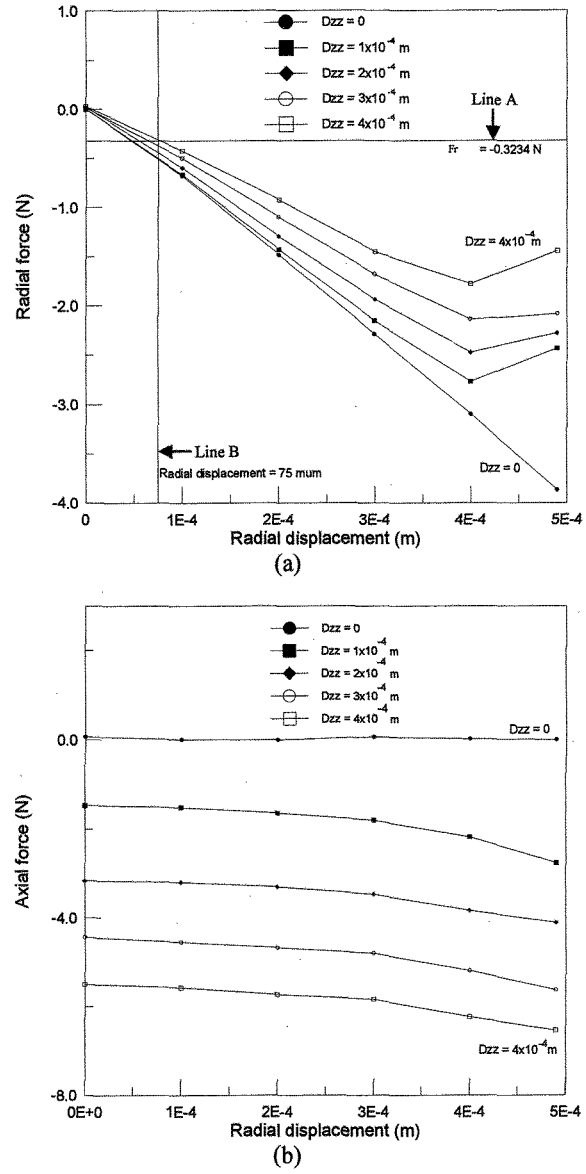

Fig. 6. (a) The radial force as a function of radial displacement of rotor. (b) The axial force as a function of radial displacement of rotor.

Thirdly, the axial force of the development system should be controlled under a proper value. The upper limit of this scope could be decided by two constrains. One is the friction torque produced by the magnetic bearing system in the dynamic state has to smaller than the ball bearing one. The other is the capacity of the thrust plate, with loading capacity defined as P, which must be smaller than 10000 kg/m^2, the maximum speed defined as V, which must be smaller than 7 m/sec, and the capacity of P×V value must be smaller than 1000 kg/(m · sec) (The coefficient of kinetic friction 0.08). Referring to the friction loss of ball bearing type spindle motor shown as Fig. 7. The cross points were the data of measurement. After curve fitting of these data points the friction equation was obtained. And it shows that friction torque is 4.209×10^{-4} Nm at the speed 3840 rpm. Then the upper limit of the axial load is equal to 10.388 N.

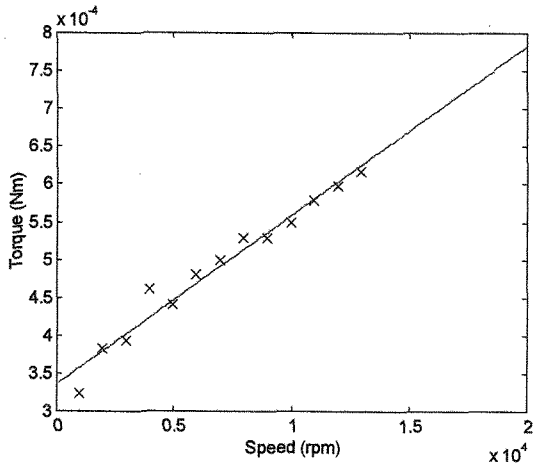

Fig. 7. Friction loss of ball bearing type spindle motor.

Suppose one third in diameter of shaft is contacted with the thrust plate. Then the V is 0.2037 m/sec and the upper limit of magnetic bearing axial force is 7.904N. From the results of calculated value, it follows that the final limit value of the axial force should be controlled smaller than 7.904N. It shows that in the stable zone of D_{zz} mentioned above, the development system has the lower friction than the ball bearing type one.

In addition to these, there is one other thing that the location of center mass of rotor is important for stabilizing the magnetic bearing system. For the analysis of a rotor system, suffering from the driving force, our laboratory had developed a dynamic equation to simulate it. Some simulation results lead to the property that the center mass of rotor should be located between the upper and lower bearings. According to this analysis the center mass of rotor was arranged below the upper magnetic bearing, but higher than the lower one. One of the simulation results is shown as Fig. 8. The center mass of rotor was located at 8 mm above the thrust plate. And the rotor can be rotated stably.

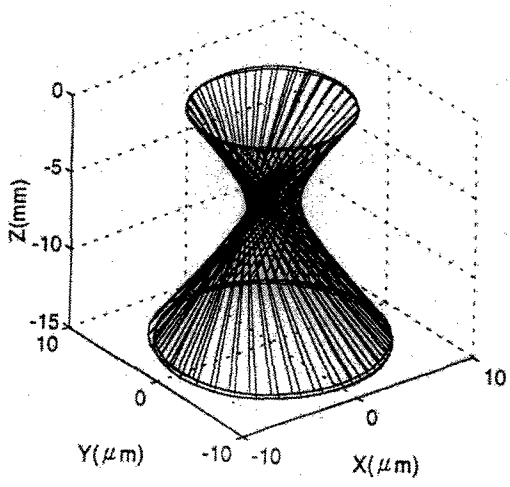

Fig. 8. Trajectory of a rotating rotor

III. Experiment Testing

Torque meter with maximum capacity 0.049 Nm and resolution 9.8×10^{-5} Nm was used to measure the friction torque loss of magnetic motor as $D_{zz} = 1\times10^{-4}$ m and ball bearing motor. The method of measuring friction torque loss generated by the objective motors, was that the motor's rotor was coupled to the shaft of the torque meter, then the motor was rotated by the torque meter to the expected four speeds 3000, 4000, 5000 and 6000 rpm. The torque loss caused by un-centering of the coupling had to be accounted. And the friction torque loss as a function of the speed was obtained.

To verify the properties of the magnetic bearing motor, three items were measured to define the performance indexes, maximum speed, current and radial run-out (which were defined as (ω_{max}, I_{max}, RRO)) when D_{zz} was fixed at four different values, 0, 1×10^{-4}, 2×10^{-4} and 3×10^{-4} m. The testing plan was constructed shown as Fig. 8. The precise laser displacement meter with the resolution 0.5 μm was used to measure the RRO. Two detectors were included in this meter. After the testing was performed, the motor was rotated at the maximum speed. The laser beam was emitted from the meter and was reflected by the rotating shaft. The detector collected the returning optical signal. Then the RRO was calculated and recorded. In order to analyze the profiles of the RRO the oscilloscope was connected to the measuring loop. The time domain of the radial run-out was obtained. By using the FFT (Fast Fourier Transform), the frequency domain of the radial run-out was measured.

For measuring the damping ratio, a shaker is included in this testing system. When magnetic motor was in the static state, an accelerometer was attached to the rotor in the radial direction. The shaker generated the input driving force and the rotor of the magnetic bearing motor was excited and vibrated. The radial acceleration of the rotor was measured by using the accelerometer and the time response of the rotor was recorded. From the frequency impulse method the damping ratio ξ was calculated by the general equation, $\xi = \delta/\omega_n \tau_d$. The δ is equal to $\ln(x_1/x_2)$, where the x_1 and x_2 are the peaks amplitudes chosen from the time response profile.

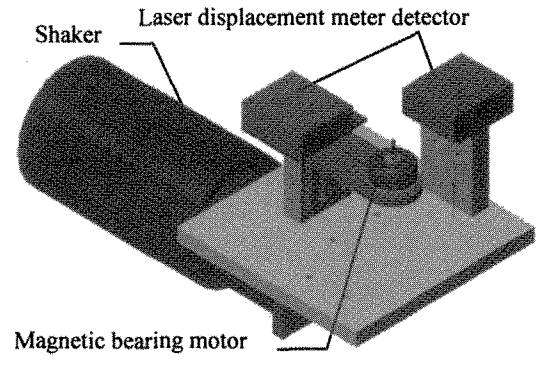

Fig. 9. Testing-plan of maximum speed, current and radial run-out.

IV. RESULTS AND DISCUSSION

The result of the friction torque loss is shown in Fig. 10. The friction torque loss increased linearly with the rising speed. For the magnetic bearing motor, the friction torque losses were 3.0×10^{-4} and 3.7×10^{-4} Nm at the rotating speed of 3000 rpm and 6000 rpm respectively. According to these two speeds, relative friction torque losses of ball bearing motor were 4.0×10^{-4} and 4.7×10^{-4} Nm. It indicates that the magnetic bearing motor has the lower friction torque loss. The result agreed with those obtained by FEA.

Two of the RRO profiles with its FFT curves are shown as Fig. 11 and Fig. 12. Fig. 11 (a) shows the radial run-out profile with RRO = 8.3×10^{-5} m (peak to peak) as D_{zz} = 0 and its FFT curve represents the dominant frequency occurs at 64 Hz (3840rpm) as shown in Fig. 11 (b). It is 41 Hz greater than natural frequency due to the natural frequency occurred at around 23 Hz. Fig. 12 (a) shows the radial run-out profile with RRO = 7.0×10^{-5} m (peak to peak) as D_{zz} = 3×10^{-4} m and its FFT curve represents the dominant frequency occurs at 64.25 Hz (3855rpm) as shown in Fig. 12 (b). It is 41.25 Hz greater than the natural frequency.

It follows from what has been discussed that in the same range of D_{zz} between zero and 3×10^{-4} m, the radial run-out of the magnetic bearing motor is smaller than 100μm. It is obvious that the shaft can be rotated without any frictional contacts in radial direction. Besides it is important that both the two FFT curves stated above, the dominant frequencies occurred at the rated speed and it is a certain level greater than the natural frequency specifies the stability of the magnetic bearing motor. Since no vibrations were observed on running the magnetic bearing through the critical speed, the design of the magnetic bearing motor is good and stable.

For D_{zz} = 0, 1×10^{-4}, 2×10^{-4} and 3×10^{-4} m, the performance indexes measured were as followed ($\omega_{max} \geq$ 3840 rpm, $I_{max} \leq$ 0.28 A, RRO $\leq$ 100 μm). Testing results of (ω_{max}, I_{max}, RRO) were arranged in the table II. The experimental data has the same agreement with the prediction of FEA.

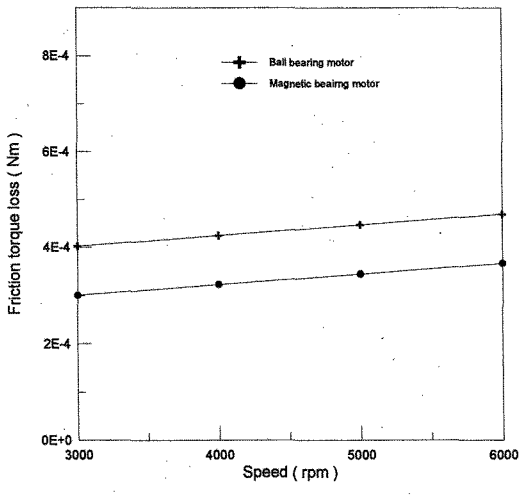

Fig. 10. Friction torque loss

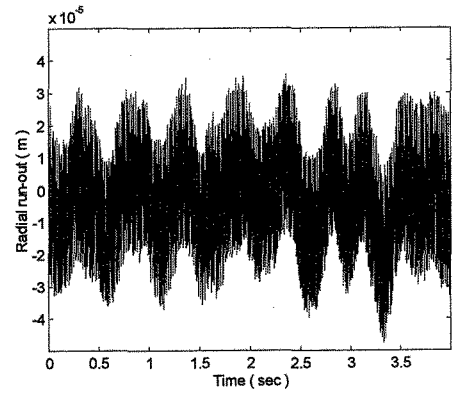

(a) Radial run-out profile

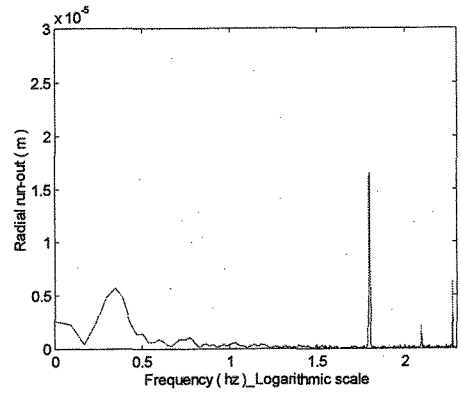

(b) FFT curve of Radial run-out profile

Fig. 11. Radial run-out profile with its FFT curve when the D_{zz} = 0.

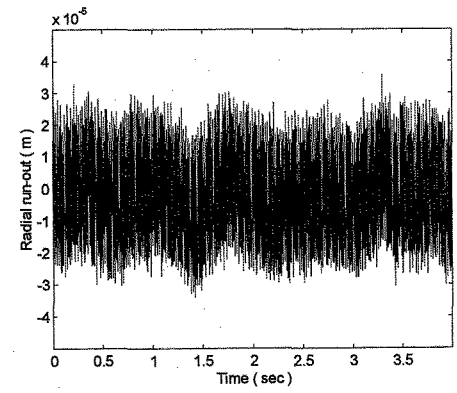

(a) Radial run-out profile

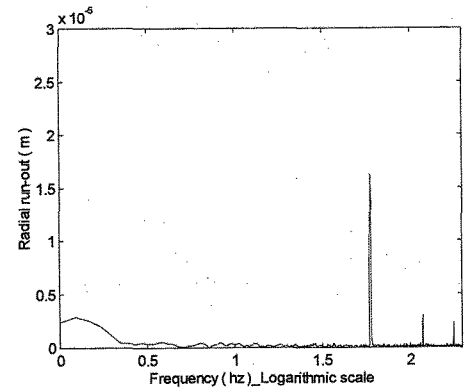

(b) FFT curve of Radial run-out profile

Fig. 12. Radial run-out profile with its FFT curve when the $D_{zz} = 3\times10^{-4}$ m.

Table II. Testing results of (ω_{max}, I_{max}, RRO).

$D_{zz}(10^{-5}m)$	ω_{max} (rpm)	I_{max} (Amp)	RRO (10^{-6}m)	State
0	3840	0.28	83	Stable
10	3870	0.28	76	Stable
20	3870	0.28	72	Stable
30	3855	0.28	70	Stable

From the data of Fig. 6 (a) and 6 (b), both the radial and axial stiffnesses of magnetic bearings can be calculated. The radial stiffness is 7508 N/m and the axial stiffness is 14764 N/m. According to Earnshaw's theorem and axial symmetry it implies that the axial stiffness should be exactly twice the radial stiffness. Comparing the FEA axial stiffness of 14764 N/m to twice the FEA radial stiffness of 7508 N/m showed that the result had the same agreement with Earnshaw's theorem 2:1 (Within 1.7 percent error).

The natural frequencies for lateral and rotational modes of the rotor are around 23Hz measured by impulse response method. The magnetic bearing motor system can be rotated successful at rated speed 3840 rpm, which is 2460 rpm above the first critical speed of 1380 rpm. The natural damping ratio in radial direction of the rotor is 0.0545. Fig. 13 shows (a) the radial free vibration history of the rotor as a function of time and (b) the radial frequency response of the rotor.

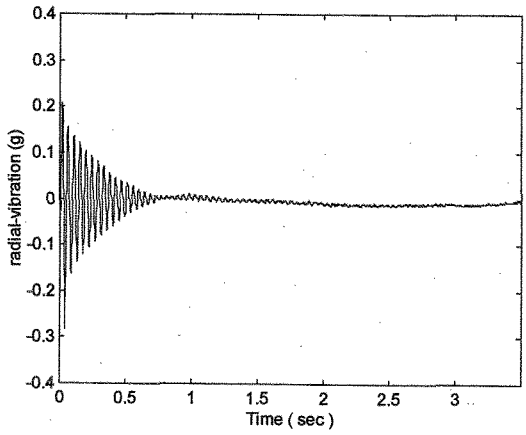

(a) Time response

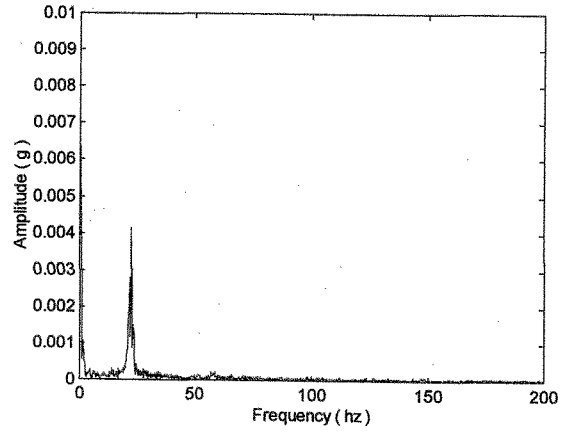

(b) Frequency response

Fig. 13. Time response and frequency response of the rotor.

V. CONSLUSIONS

An innovative magnetic bearing motor has been developed successfully. The running current is around 0.28 A, the maximum speed is around 3840 rpm. The radial run-out obtained is smaller than 100 μm. The shaft can be rotated without any frictional contacts in radial direction. Lower friction torque loss 1.0×10^{-4} Nm smaller than that of ball bearing motor is obtained. The developed magnetic bearing may be effectively applied as a long life and low noise bearing of the spindle motor.

Comparing the FEA axial stiffness of 14764 N/m to F.E.A radial stiffness of 7508 N/m showed that the result has the same agreement with Earnshaw's theorem 2:1 (within 1.7 percent error)

The natural frequencies for lateral and rotational modes of the rotor are around 23 Hz measured by impulse response method. It is 41 Hz lower the rated speed 64 Hz, and the system resonance is avoided. The natural damping ratio in radial direction of the rotor is 0.0545. The magnetic bearing spindle motor will be useful for data storage applications.

REFERENCES

[1] John C. Dunfield, Kamran Oveyssi and Gunter K. Heine, "Passive Magnetic Bearing for A Spindle Motor", 5,619,083, U.S., Apr. 8, 1997.

[2] Alexei V. Filatov, Eric H. Maslen, "Passive magnetic Bearing for Flywheel Energy Storage Systems", IEEE Trans. Magn, Vol.37, pp. 3919-3924 (2001).

[3] Mochimitsu Komori; Taku Hamasaki, "Improvement of Dynamics for a Supercoductivity", IEEE. Applied Superconductivity, Vol. 37, pp. 158-163 (1998).

[4] Murakami Tsutomu, "Passive Bearing Device", 4,290,609, J.P., Oct. 15, 1992.

[5] Alex Horng, " Brushless D.C. Motor Assembly ", 6,097,120, U.S., Aug. 1, 2000.

[6] S. Earnshaw, Trans. Cambridge Philisophical Society, 7, 97-112 (1839).

(Received October 8, 2003; Accepted February 5, 2004)